

Article

# Interaction of Extracellular Vesicles with Si Surface Studied by Nanomechanical Microcantilever Sensors

Stefania Federici <sup>1,2,\*</sup>, Andrea Ridolfi <sup>1</sup>, Andrea Zandrini <sup>3</sup>, Annalisa Radeghieri <sup>3,4</sup>,  
Elza Bontempi <sup>1,2</sup> , Laura E. Depero <sup>1,2</sup> and Paolo Bergese <sup>2,3,4</sup>

<sup>1</sup> Department of Mechanical and Industrial Engineering, University of Brescia, 25123 Brescia, Italy; a.ridolfi@studenti.unibs.it (A.R.); elza.bontempi@unibs.it (E.B.); laura.depero@unibs.it (L.E.D.)

<sup>2</sup> Consorzio Interuniversitario Nazionale per la Scienza e Tecnologia dei Materiali (INSTM), 50121 Firenze, Italy; paolo.bergese@unibs.it

<sup>3</sup> Department of Molecular and Translational Medicine, University of Brescia, 25123 Brescia, Italy; andreazandrini@gmail.com (A.Z.); annalisa.radeghieri@unibs.it (A.R.)

<sup>4</sup> Consorzio Interuniversitario per lo Sviluppo dei Sistemi a Grande Interfaccia (CSGI), 50019 Sesto Fiorentino, Italy

\* Correspondence: stefania.federici@unibs.it; Tel.: +39-030-371-5574

Received: 9 February 2018; Accepted: 6 March 2018; Published: 9 March 2018

**Abstract:** We report on the interaction of small (<150 nm) extracellular vesicles (EVs) with silicon surface. The study is conducted by leveraging Si nanomechanical microcantilever sensors actuated in static and dynamic modes, that allow tracking of EV collective adsorption energy and adsorbed mass. Upon incubation for 30 min at about 10 nM concentration, EVs isolated from human vascular endothelial cell (HVEC) lines form a patchy layer that partially covers the Si total surface. Formation of this layer releases a surface energy equal to  $(8 \pm 1) \text{ mJ/m}^2$ , typical of weak electrostatic interactions. These findings give a first insight into the EV-Si interface and proof the possibility to realize new hybrid biointerphases that can be exploited as advanced models to investigate properties of biological membranes and/or biosensing platforms that take advantage of biomolecules embedded/supported in membranes.

**Keywords:** nanomechanical sensors; extracellular vesicles; surface stress; hybrid biointerphases

## 1. Introduction

Extracellular vesicles (EVs) are natural cell-derived nanoparticles containing bioactive proteins, nucleic acids, and metabolites, which are newly recognized as universal agents of intercellular and inter-organismal communication, in both normal and pathological processes [1–3]. This poses on EVs great expectations as means for precision diagnostics [4] and therapeutics [5,6], now supported by the first early phase [7] clinical-trials, encompassing oncology, immunology, tissue regeneration, neurodegenerative disorders (e.g., Alzheimer’s disease), and infectious and parasitic diseases (e.g., diphtheria and malaria).

However, full understanding and control of the biology of EVs and the physical basis of their interactions are still unmet needs that hamper EV manipulation (including chemical or biological modification) and in turn effective translation to the clinic [8]. For instance, the colloidal and interfacial properties of EVs have started to be tackled only very recently [9–11], and the mechanisms that govern direct interaction of EVs with synthetic surfaces is mostly unexplored.

In this study, we present a first attempt to characterize the interaction of nanosized (also referred as small [12]) EVs with Si surface by nanomechanical microcantilever (MC) biosensors [13]. The surface was selected as it is the most representative inorganic solid surface among the ones employed in biological applications, spanning from biosensors [14,15] to organoid-on-a-chip [16]. MC biosensors

were chosen for their ability to probe mass adsorption and interaction energetics at the solid–liquid interface of minute volumes of synthetic liposomes [17,18], comparable with standard EV formulations obtained from biological fluids or cell culture media, which are typically 100  $\mu$ L solution volumes at few nM EV concentration (see for example [9]). Small EVs were isolated from an immortalized cell line of human vascular endothelial cell (HVEC) that is routinely used as model of EV-secreting cells, since it produces a good amount of highly pure exosomes compared to other cell types [19].

## 2. Materials and Methods

### 2.1. Materials

All reagents were purchased from Sigma-Aldrich (St. Louis, MO, USA) unless otherwise specified.

### 2.2. Extracellular Vesicles Separation and Characterization

HVEC cells were grown in complete Roswell Park Memorial Institute (RPMI) 1640 medium, supplemented with 10% fetal bovine serum, 1% Penicillin/Streptomycin and 1% Glutamine, at 37 °C, 5% CO<sub>2</sub>, until 80% confluence was reached [19,20]. Complete medium was removed and cells were rinsed thrice with sterile phosphate buffer saline (PBS). Ten mL of serum free RPMI 1640, supplemented with 1% penicillin/streptomycin and 1% glutamine, was added to each plate. A serial centrifugation protocol previously described [21] was used to isolate EVs produced by  $2 \times 10^7$  cells from serum free medium, after 24 h incubation. The quantity of isolated EVs obtained by serum-free culture medium is greatly increased while retaining EV biophysical and size properties [22]. Before further analysis, EV pellets were resuspended in 50  $\mu$ L PBS 10 mM supplemented with 1:1000 protease inhibitor cocktail. EV preparation purity was graded by a colorimetric nanoplasmonic (CONAN) assay [9], and related UV–vis spectroscopy measurements performed by a EnSight multimode plate reader (Perkin Elmer, Waltham, Massachusetts, United States). EV titration was performed as described in [23]; the calibration line was built with POPC (1-palmitoyl-2-oleoyl-sn-glycero-3-phosphocholine, Avanti Polar Lipids, Alabaster, AL, USA) liposomes of about 60 nm size.

EV biochemical characterization was performed by western blot [24]. For the analysis sodium dodecyl sulfate (SDS) sample buffer was added to isolated EVs and samples were boiled 5 min at 95 °C. Samples were electrophoresed and analyzed with rabbit anti-GM130 (Rockville, MD, USA), mouse anti-Alix (Santa Cruz Biotechnology, Dallas, TX, USA), mouse anti-Hsp 70 (Enzo Life Science, Lausen, Switzerland), mouse anti-CD63 (Merck-Millipore, Darmstadt, Germany), mouse anti-annexin-V (Santa Cruz Biotechnology). HVEC lysate was used as a control (15  $\mu$ g of proteins).

For atomic force microscope (AFM) imaging, EV samples were diluted 1:10 in Milli-Q water. Measures of 7–10  $\mu$ L were spotted on mica substrates—freshly cleaved with the help of adhesive tape to produce clean, atomically flat surfaces (Grade V-1, thickness 0.15 mm, size 10  $\times$  10 mm—and let dry at room temperature [25]. Samples were then analyzed with a NaoAFM microscope (Nanosurf, Liestal, Switzerland), equipped with MultiGD-G probes (BudgetSensors, Sofia, Bulgaria) and run in dynamic mode. Scanning parameters were tuned according to instrument and probes' manufacturers. Images were processed using WSxM 5.0, a freeware scanning probe microscopy software [26].

For MC experiments, pellets were resuspended in 300  $\mu$ L of PBS. The scheme of the experimental process is sketched in Figure 1.

### 2.3. Microcantilever Experiments

The interaction of EVs and MCs was probed by the Cantisens Research platform (Concentris GmbH, Basel, Switzerland), that allows simultaneous experiments in both static and dynamic mode. The instrument is equipped with a microfluidic system to deliver the liquid and for all the experiments the flux rate was set to 0.42  $\mu$ L/s. The readout of the deflection of each individual MC is performed simultaneously by multiple lasers focused to the end of the MC and the temperature of the

measurement chamber was set at 25 °C. MC arrays architecture consists of eight Si MCs with the top faces coated by a 20 nm Au thin film.

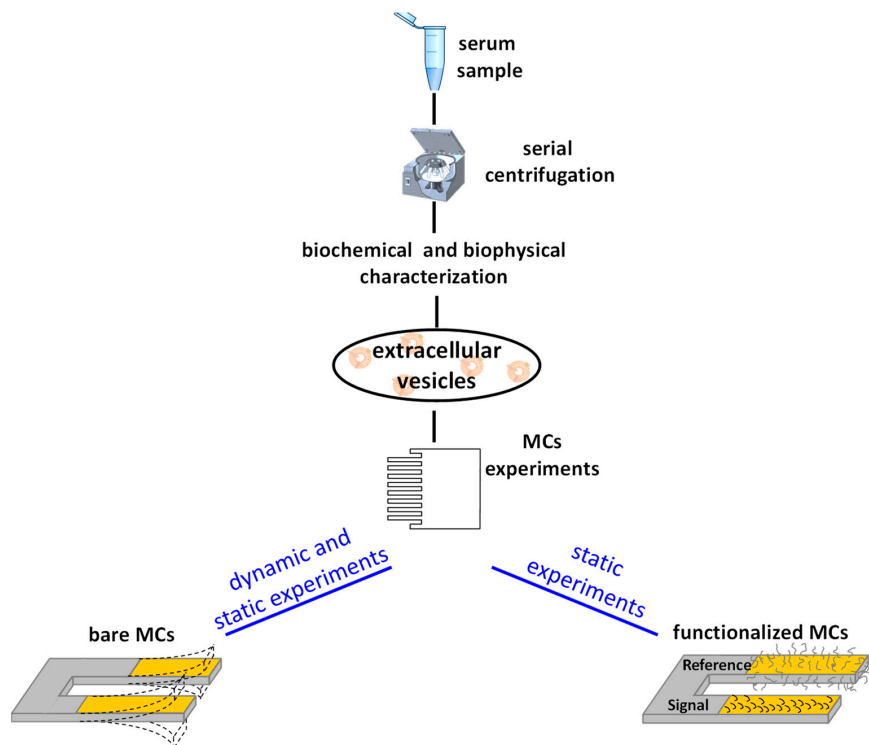


**Figure 1.** Protocol of the experimental steps. Scheme of the experimental process.

For experiments in static mode, arrays of eight rectangular MCs of the same size were employed, namely 500 μm long, 100 μm wide, and 1 μm thick (Concentris GmbH, Basel, Switzerland). Four of them used as internal reference were passivated with polyethylene glycol, 3400 Da (PEG 3k) in a capillary system for 3 h. The other four MCs were passivated with 6-mercapto1-hexanol in capillary system for 3 h. MC deflection can be related to the change in surface stress by Stoney’s equation [27]

$$\Delta\sigma = \frac{E t^2 \Delta z}{4 l^2(1 - \nu)} \tag{1}$$

where *t* is the thickness of the cantilever, *l* is the length, *E* is Young’s modulus (*E* = 169 GPa), and *ν* the Poisson’s ratio (0.25 for rectangular MC).

For experiments in dynamic mode, MCs were chosen with different lengths, and thus resonance frequencies (Concentris GmbH), in order to minimize mechanical crosstalk. The resonance frequency steps between MCs are 26 kHz on the first mode (according to Sader Inviscid Model [28]). MCs are 100 μm in width and 7 μm thick, the lengths are 212, 315, 249, and 500 nm repeated twice, and density of 2330 kg/m<sup>3</sup>. The determination of the added mass is calculated according to [28]. The assumptions consider the effect of the EV deposition purely mass-related and negligible the contribution in the change of spring constant. This is a good approximation for the adsorption of a soft layer of biomolecules onto the MC surface, as reported in [29,30]. Density and volume are considered constant over the whole experiment and for all samples. For further details, please refer to [28,29]. Knowing the resonance frequency before (*f<sub>a</sub>*) and after (*f<sub>b</sub>*) the adsorption of EVs, the adsorbed mass is calculated as

$$\Delta m = G_p^2 C_n^2 E \left( \frac{1}{f_b^2} - \frac{1}{f_a^2} \right) \tag{2}$$

where  $G_p$  is an empirical coefficient that takes into account the differences between the experimental and ideal mechanical behavior of a microcantilever (internal defects and geometrical differences from the nominal values),  $C_n$  is equal to  $\beta_n^2/2\pi\sqrt{3}$ , where  $\beta_n$  are the solutions of the equation  $\cos \beta_n l \cosh \beta_n l + 1 = 0$ , and  $E$  is the young modulus of the microcantilever [31].

Before each experiment, MCs were immersed in acetone for 30 min and cleaned by UV/ozone plasma (PSD-UVT, Novascan Technologies, Boone, IA, USA) for 30 min. In all the experiments, the MCs were stabilized in PBS 10 mM for about 3 h before the injection of EV solution in PBS 10 mM. After injection, the EV solution was allowed to flow in the measurement chamber for about 2 min and then the flow stopped for about 30 min, in order to allow interaction equilibrium to be attained.

### 3. Results and Discussion

#### 3.1. Extracellular Vesicles Characterization

EVs were purified from conditioned medium of HVEC cell line. Results for the characterization of EV samples are shown in Figure 2. Purity of EV samples with respect to exogenous single and aggregated protein contaminants and titration was determined by CONAN assay. The assay, based on a 3 nM dispersion of 15 nm gold nanoparticles (AuNPs), grades the purity of the preparation by color change. Change is visible by eye and can be quantified through the aggregation index (AI) which is inversely proportional to the preparation purity. AI is defined as the ratio between the localized surface plasmon resonance (LSPR) absorbance at 519 nm and 650 nm, and is determined by conventional UV-vis spectrometry. The determined AI for the used preparation resulted below 25% of the AI of the dispersed AuNPs (Figure 2A), corresponding to a contaminant content  $<10 \text{ ng}/\mu\text{L}$  (according to the calibration reported in Ref. [9]), that is a high purity preparation.

Figure 2B shows the western blot analysis of the EV samples. The conventional EV markers Alix, HSP70, CD63, and annexin V were tested, and all of them were found to be expressed in the EV population and in the parent cells. GM130 (a Golgi-related protein) was used as a negative control, that is considered to be not expressed in EVs, and it confirms the absence of cell debris. Due to the intrinsic problem related to the quantification of protein content in EVs, the western blot must be interpreted in a qualitative way. The only purpose is to check the presence of typical EV markers in the EV preparations and ensure their presence in the parent cells.

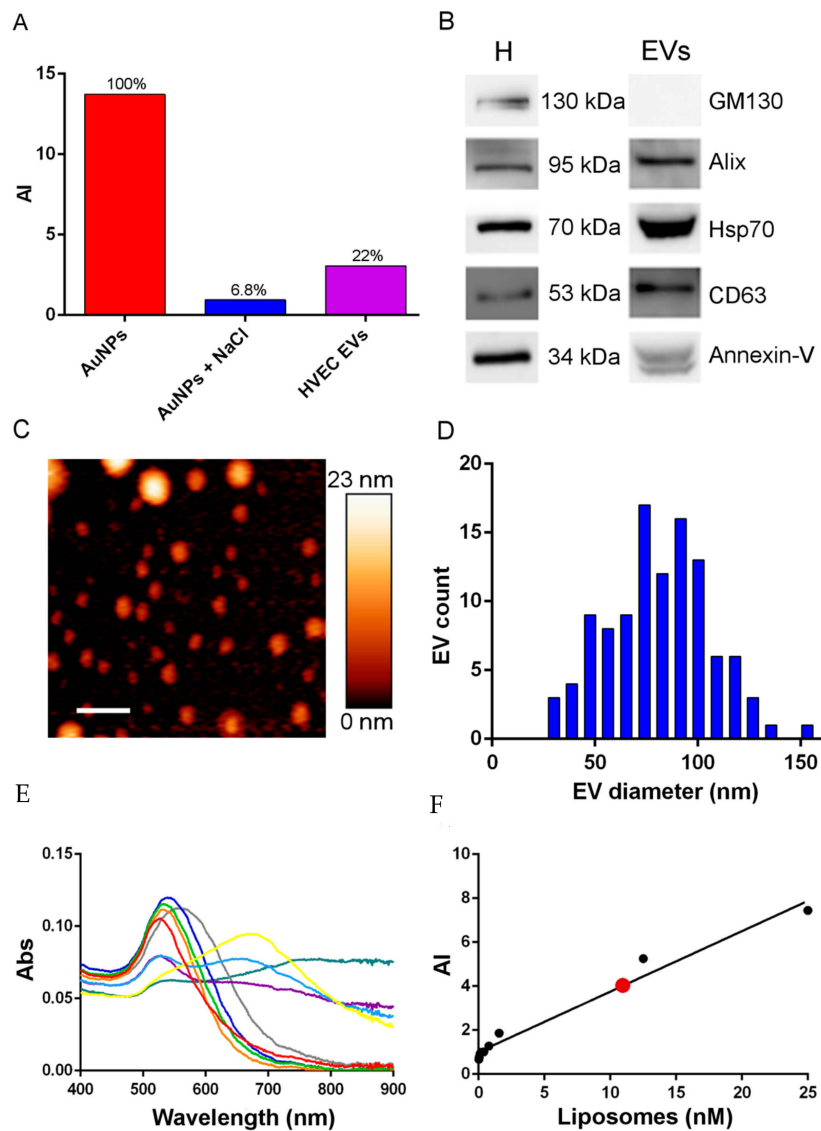
The morphological characterization of the EVs was carried out by means of AFM in dried ambient conditions. A representative image is displayed in Figure 2C. The nanometer flatness of the background confirms absence of exogenous contaminants [32]. Figure 2D reports the bar chart of EV size distribution, showing EVs with a size ranging from 30 nm to 160 nm, with a peak at the size of 65–75 nm.

Figure 2E,F show the EV samples titration results, obtained conducting the experiments. POPC liposomes are used as synthetic, convenient mimic of EVs to create the calibration line used for EV titration. Figure 2E reports the UV-vis spectra of the POPC liposome standards used to create the calibration line reported in Figure 2F. Each standard is prepared by adding a fixed amount of AuNPs to liposome solutions at decreasing total titers. The redshift of the AuNP spectra is directly proportional to liposome molar concentration. Therefore, the lower is the liposome molar concentration, the greater is the redshift and the lower is the AI. The same applies to pure EV samples with unknown concentration. The red dot represents the calibration intercepts of the EV preparations used for the experiments, which resulted in a final molar concentration around 10 nM.

#### 3.2. Interaction between Extracellular Vesicles and Microcantilevers

Microcantilevers are nanomechanical based sensors designed to measure surface stress changes induced by biomolecular recognition and adsorption occurring on their surface (static mode) and/or contemporarily measure the resonance frequency shifts due to the related mass change (dynamic mode) [13]. These peculiar characteristic prompted successful application of MC sensors, and other

tensiometric biosensors to label-free study of molecular collective surface nanomechanics [33–36], opening new insights in surfaces confined molecular transformations and machines [32,37–40], up to single cell investigation [41–43].



**Figure 2.** Characterization of extracellular vesicles (EVs) samples. (A) Aggregation index (AI) of EV preparation. AI is inversely proportional to the preparation purity grade; (B) western blot of EV samples and parent cells (H) with the EV markers Alix, CD63, HSP70, annexin V, and GM130 as negative control; (C) Atomic Force Microscopy (AFM) image of EVs (scale bar = 200 nm) and (D) EV size distribution. A total of 108 objects with a size between 30 nm and 160 nm were analyzed; (E,F) Colorimetric nanoplasmonic (CONAN) analysis of molar concentration of EVs. Refer to the main text for the details.

Experiments exploiting static deflection of MC beams are reported in literature to study the chemi- or physisorption of synthetic lipid bilayer on a cantilever surface, on either gold (Au) or silicon dioxide (SiO<sub>2</sub>) surfaces [17,18]. Moreover, measurements of the resonance frequency shift induced upon phospholipid vesicle adsorption on oscillating cantilevers immersed in a liquid have been described [30]. In the case of static deflection, the bending of the cantilever is caused by the difference in the surface stress between the upper and lower surface. Usually, to reach this asymmetry,

the cantilevers are Au coated on one side and show a Si surface on the opposite side. The two surfaces allow selective use of either thiol chemistry to functionalize/passivate the Au side or silane chemistry for the Si side [44]. Typical experiments exploit the well-known fact that liposomes readily adsorb and fuse on glass or silicon dioxide, giving rise to extended, homogeneous lipid double layers [45,46]. The common functionalization choice is then to protect the Au side of cantilevers and drive the vesicles fusion primarily on the SiO<sub>2</sub> surface [18]. Stability of liposomes on Au surfaces is instead not well understood: electrostatic (image-charge) attraction should provide strong adhesion leading to vesicles rupture and bilayer formation, yet adsorbed lipids exhibit negligible lateral diffusion. It is demonstrated that vesicles partially fuse, to some extent, on gold, but the resulting membrane lacks long-range lateral mobility over the time scale of several hours [47,48].

In the first set of experiments, we addressed the interaction of the EVs with the Si surface. We employed the array of eight replicate MCs. Four of them used as internal reference and therefore with both faces passivated with PEG to prevent vesicles fusion [49] and protein adsorption [50]. The other four MCs instead had the Au surface passivated with 6-mercapto-1-hexanol, to drive and limit EVs to interact with the Si surface (Figure 3A). The MCs mean differential deflection signal between the four active MCs absolute deflection and the four reference MCs absolute deflection is reported in Figure 3B together with the errors (as standard deviation of the mean) at selected points.

The first part of the signal is characterized by typical background noise deflection of few nm. When the EV solution is injected into the measurement chamber, the equilibrium interaction between the EVs and the MCs drives significant and chaotically oscillating deflections up to hundreds of nm. This behavior characterizes the whole 30 min the MCs are incubated with the EV solution (stopped flow), and is in agreement to what previously observed with liposomes [17]. When the flow is restarted and the solution is replaced by the pure buffer, excess and weakly adsorbed EVs are washed away and the MCs stabilize with an upward differential deflection of  $\Delta z = (38 \pm 5)$  nm, which probes the formation of a stable EV layer. By substituting  $\Delta z$  into Equation (1) we learn that the layer formation involves a surface work that appears as a surface stress change of  $\Delta\sigma = (8 \pm 1)$  mJ/m<sup>2</sup>. This result is about half the value reported in the literature for the surface stress measured for the formation of supported lipid bilayer (SLB) on SiO<sub>2</sub> surface from POPC liposomes [17,18]. This indicates that the formed layer is not continuous and/or that the formation of the EV layer is less energetic. Very likely a combination of both.

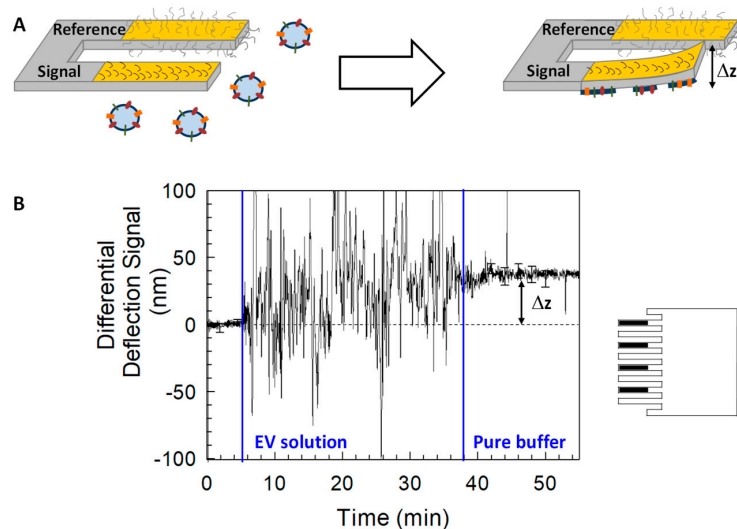


**Figure 3.** Static microcantilever (MC) experiments. (A) Scheme of MCs and their deflection due to the interaction between the EVs and their silicon bottom face; (B) MCs mean differential deflection driven by the interaction of the EVs with the MCs. The error bars represent the standard deviation of the mean.

To explore the hypotheses formulated after the results of the first set of experiments, we exploited the dynamic mode of MCs actuation, measuring the mass contribution of the EV layer during the EV interaction with the MC surface.

For this set of experiments, we used bare MCs without any passivation, in order to maximize the adsorbed EVs and obtain significant results with respect to the limit of detection (viz. the largest frequency shift achievable).

Figure 4B shows the resonant frequency signal of a representative MC. After injection, the EV solution was allowed to flow in the measurement chamber for about 2 min, corresponding to the first peak in the frequency signal. Then the flow was stopped for about 30 min allowing equilibrium interaction of the EVs with the MCs. During this period the frequency signal decreases due to the increased adsorbed mass. After this period the flow was restarted, corresponding to the second peak in the signal, until the buffer has completely removed the excess and weakly adsorbed EVs and the signal reaches its final value. Three replicates of this experiment were performed with three different MC arrays. The value of added mass was determined by Equation (2) yielding a mean value of  $m = (110 \pm 40) \text{ ng/cm}^2$ .

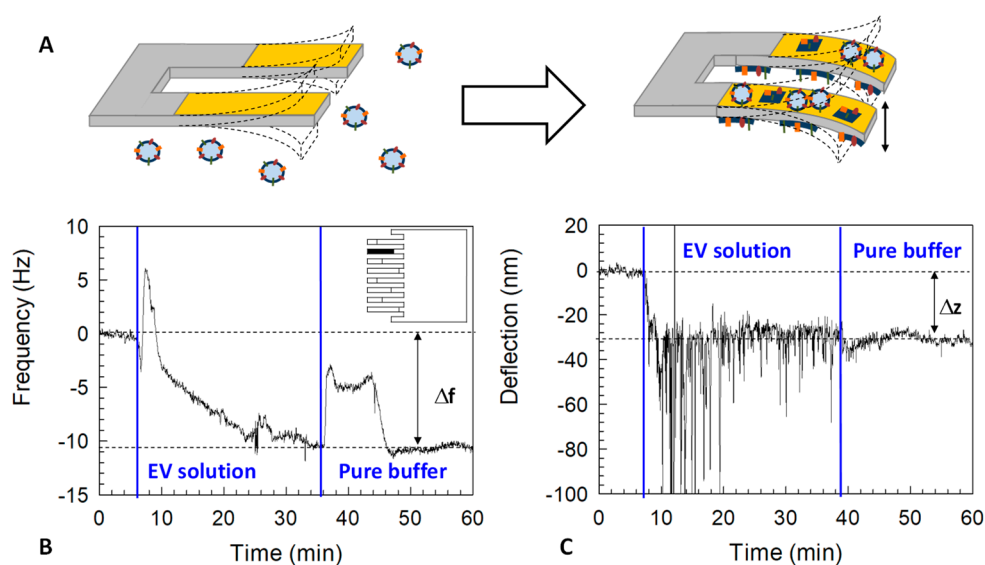


**Figure 4.** Simultaneous MCs experiments in static and dynamic mode. (A) Scheme of the interaction between MCs and EVs; (B) representative MC frequency signal due to the interaction of EVs and MC surfaces; (C) absolute deflection signal of the MC of panel B.

The interpretation of this measured added mass can be assisted by calculating a theoretical value of added mass. Let us consider a MC surface occupied by a continuous double layer of phospholipids, with a single phospholipid head of  $0.7 \text{ nm}^2$ , a mass of  $1.26 \times 10^{-24} \text{ kg}$  and a packing factor onto the surface between 0.5 and 1. The theoretical estimation of the value can range between  $180 \text{ ng/cm}^2$  and  $360 \text{ ng/cm}^2$ .

This calculation underestimates the real value, due to the following assumptions: (a) it does not take into account the contribution of the proteins that EVs harbor on the surface, and (b) it assumes similar contribution in weight of the two faces of the MC, neglecting the possibility to have intact vesicles on the Au surface that would pack in the same surface area, with a  $> 5$  times higher mass. Taking into account these considerations, we expected an experimental value higher than the theoretical one, instead the result was slightly lower. This can be ascribed to the formation of non-continuous layers of EVs on the surface, maybe both on the Au and Si faces, supporting the results indicated by the first set of experiments.

This conclusion is further supported by the final absolute deflections of the MCs actuated in dynamic mode (Figure 4C). In this configuration, the system measures both the resonance frequency shift induced upon EV adsorption on MCs and the bending of the MCs due to the surface stress change. Our particular experimental conditions (without any passivation) allows a direct comparison between the surface stress generated on the Au and Si surfaces.

In this configuration, the absolute deflection signal considered at equilibrium is  $\Delta z = (-41 \pm 6)$  nm. Substitution of this value into Equation (1) indicates that the surface stress exerted by the EVs adsorbed on the top Au face is higher than the one exerted by the EVs adsorbed onto the Si face by  $\Delta\sigma = (28 \pm 4)$  mJ/m<sup>2</sup>. This result can be discussed by taking into account the results reported in the literature about deflection signals upon injection of liposomes onto functionalized SiO<sub>2</sub> and Au surfaces [18]. As already discussed, Liu and co-workers demonstrated that upon incubation with POPC liposomes, a SLB forms on the SiO<sub>2</sub> surface, resulting in a positive deflection due to a compressive stress of  $\Delta\sigma = (17.0 \pm 1.4)$  mJ/m<sup>2</sup>. Instead, they also showed that intact liposomes adsorb onto the Au surface of the MC, exerting a compressive stress  $\Delta\sigma = (98 \pm 7)$  mJ/m<sup>2</sup>. That is, intact vesicles adsorb on the Au surface and generate a surface stress about five times larger than the one generated by SLB formation on the Si surface.

This new result suggests that EVs could partially fuse also on the Au surface, generating a lower surface stress than in case of intact vesicles adsorbing on the surface, opening new possibilities for biological applications of EVs in the field of biosensors and organoids on-a-chip.

#### 4. Conclusions

Microcantilever sensors were used to study the interaction of small (<150 nm) EVs isolated from HVEC cell lines. We found that upon incubation for 30 min at about 10 nM concentration this EV population adsorb onto Si surface releasing a surface energy, in the form of exerted surface stress, equal to  $(8 \pm 1)$  mJ/m<sup>2</sup>. This energy, which falls in the range of weak electrostatic interactions, has about half the value of the energy involved in the formation of SLBs from POPC liposomes, suggesting the formation of an EVs layer, which however is discontinuous and/or involves less energy. Formation of a patchy layer that partially covers the Si total surface is also supported by the final measured absolute amount of adsorbed mass, which is lower than the minimum nominal mass expected from the formation of a uniform SLB. Further studies varying EV concentrations and using complementary techniques [51] to characterize the formation pathway and properties of these EV layers and the conditions and possibility under which they may eventually take the form of a continuous SLB are in progress.

While spreading of synthetic liposomes and proteoliposomes on flat surfaces to form SLBs is extensively studied [52,53], the present work is among the first attempts to extend this research to EVs. EV layers may be used as novel accurate models to investigate properties of biological membranes. Finally, the reported findings also originally contribute to the effort to prepare biosensing platforms that take advantage of biomolecules embedded/supported in membranes [54], circumventing complex time-consuming procedures required to prepare artificial vesicles [55,56].

**Acknowledgments:** The authors acknowledge the funding of the Italian MIUR (Ministero dell'Istruzione, dell'Università e della Ricerca) for financial support of ex 60%. They also wish to thank Debora Berti and Costanza Montis for fruitful discussions, and Orietta Salvucci for supplying HVEC cell lines.

**Author Contributions:** Stefania Federici and Paolo Bergese conceived and designed the experiments. Stefania Federici, Andrea Ridolfi, Andrea Zandrini, and Annalisa Radeghieri performed the experiments. Elza Bontempi and Laura E. Depero contributed reagents/materials/analysis tools and contributed to design the experiments. Stefania Federici and Paolo Bergese wrote the paper. All authors discussed the results and contributed to the final manuscript.

**Conflicts of Interest:** The authors declare no conflict of interest.

## References

1. Yanez-Mo, M.; Siljander, P.R.; Andreu, Z.; Zavec, A.B.; Borràs, F.E.; Buzas, E.I.; Buzas, K.; Casal, E.; Cappello, F.; Carvalho, J.; et al. Biological properties of extracellular vesicles and their physiological functions. *J. Extracell. Vesicles* **2015**, *4*, 27066. [[CrossRef](#)] [[PubMed](#)]
2. Nolte-'t Hoen, E.; Cremer, T.; Gallo, R.C.; Margolis, L.B. Extracellular vesicles and viruses: Are they close relatives? *Proc. Natl. Acad. Sci. USA* **2016**, *113*, 9155–9161. [[CrossRef](#)] [[PubMed](#)]
3. Deatherage, B.L.; Cookson, B.T. Membrane Vesicle Release in Bacteria, Eukaryotes, and Archaea: A Conserved yet Underappreciated Aspect of Microbial Life. *Infect. Immun.* **2012**, *80*, 1948–1957. [[CrossRef](#)] [[PubMed](#)]
4. De Toro, J.; Herschlik, L.; Waldner, C.; Mongini, C. Emerging roles of exosomes in normal and pathological conditions: New insights for diagnosis and therapeutic applications. *Front. Immunol.* **2015**, *6*, 203. [[CrossRef](#)] [[PubMed](#)]
5. Andaloussi, S.E.L.; Mäger, I.; Breakefield, X.O.; Wood, M.J.A. Extracellular vesicles: Biology and emerging therapeutic opportunities. *Nat. Rev. Drug Discov.* **2013**, *12*, 347–357. [[CrossRef](#)] [[PubMed](#)]
6. Marcilla, A.; Martin-Jaular, L.; Trelis, M.; de Menezes-Neto, A.; Osuna, A.; Bernal, D.; Fernandez-Becerra, C.; Almeida, I.C.; Del Portillo, H.A. Extracellular vesicles in parasitic diseases. *J. Extracell. Vesicles* **2014**, *3*, 25040. [[CrossRef](#)] [[PubMed](#)]
7. Fais, S.; O'Driscoll, L.; Borrás, F.E.; Buzas, E.; Camussi, G.; Cappello, F.; Carvalho, J.; Cordeiro da Silva, A.; Del Portillo, H.; El Andaloussi, S.; et al. Evidence-Based Clinical Use of Nanoscale Extracellular Vesicles in Nanomedicine. *ACS Nano* **2016**, *10*, 3886–3899. [[CrossRef](#)] [[PubMed](#)]
8. Ingato, D.; Lee, J.U.; Sim, S.J.; Kwon, Y.J. Good things come in small packages: Overcoming challenges to harness extracellular vesicles for therapeutic delivery. *J. Control. Release* **2016**, *241*, 174–185. [[CrossRef](#)] [[PubMed](#)]
9. Maiolo, D.; Paolini, L.; Di Noto, G.; Zendrini, A.; Berti, D.; Bergese, P.; Ricotta, D. Colorimetric Nanoplasmonic Assay To Determine Purity and Titrate Extracellular Vesicles. *Anal. Chem.* **2015**, *87*, 4168–4176. [[CrossRef](#)] [[PubMed](#)]
10. Rupert, D.L.M.; Claudio, V.; Lasser, C.; Bally, M. Methods for the physical characterization and quantification of extracellular vesicles in biological samples. *Biochim. Biophys. Acta* **2016**, *1861*, 3164–3179. [[CrossRef](#)] [[PubMed](#)]
11. Khatun, Z.; Bhat, A.; Sharma, S.; Sharma, A. Elucidating diversity of exosomes: Biophysical and molecular characterization methods. *Nanomedicine* **2016**, *11*, 2359–2377. [[CrossRef](#)] [[PubMed](#)]
12. Mateescu, B.; Kowal, E.J.; van Balkom, B.W.; Bartel, S.; Bhattacharyya, S.N.; Buzás, E.I.; Buck, A.H.; de Candia, P.; Chow, F.W.; Das, S.; et al. Obstacles and opportunities in the functional analysis of extracellular vesicle RNA—An ISEV position paper. *J. Extracell. Vesicles* **2017**, *6*, 1286095. [[CrossRef](#)] [[PubMed](#)]
13. Arlett, J.L.; Myers, E.B.; Roukes, M.L. Comparative advantages of mechanical biosensors. *Nat. Nanotechnol.* **2011**, *6*, 203. [[CrossRef](#)] [[PubMed](#)]
14. Bergese, P.; Cretich, M.; Oldani, C.; Oliviero, G.; Di Carlo, G.; Depero, L.E.; Chiari, M. Advances in parallel screening of drug candidates. *Curr. Med. Chem.* **2008**, *15*, 1706–1719. [[CrossRef](#)] [[PubMed](#)]
15. Homola, J. Surface plasmon resonance sensors for detection of chemical and biological species. *Chem. Rev.* **2008**, *108*, 462–493. [[CrossRef](#)] [[PubMed](#)]
16. Skardal, A.; Shupe, T.; Atala, A. Organoid-on-a-chip and body-on-a-chip systems for drug screening and disease modeling. *Drug Discov. Today* **2016**, *21*, 1399–1411. [[CrossRef](#)] [[PubMed](#)]
17. Pera, I.; Fritz, J. Sensing Lipid Bilayer Formation and Expansion with a Microfabricated Cantilever Array. *Langmuir* **2007**, *23*, 1543–1547. [[CrossRef](#)] [[PubMed](#)]
18. Liu, K.W.; Biswal, S.L. Using Microcantilevers to Study the Interactions of Lipid Bilayers with Solid Surfaces. *Anal. Chem.* **2010**, *82*, 7527–7532. [[CrossRef](#)] [[PubMed](#)]
19. Di Noto, G.; Paolini, L.; Zendrini, A.; Radeghieri, A.; Caimi, L.; Ricotta, D. C-src Enriched Serum Microvesicles Are Generated in Malignant Plasma Cell Dyscrasia. *PLoS ONE* **2013**, *5*, e70811. [[CrossRef](#)] [[PubMed](#)]
20. Zadeh, M.S.; Kolb, J.P.; Geromin, D.; D'Anna, R.; Boulmerka, A.; Marconi, A.; Dugas, B.; Marsac, C.; D'Alessio, P. Regulation of ICAM-1/CD54 expression on human endothelial cells by hydrogen peroxide involves inducible NO synthase. *Leukoc. Biol.* **2000**, *67*, 327–334. [[CrossRef](#)]

21. Di Noto, G.; Chiarini, M.; Paolini, L.; Mazzoldi, E.; Giustini, V.; Radeghieri, A.; Caimi, L.; Ricotta, D. Immunoglobulin free light chains and GAGs mediate multiple myeloma extracellular vesicles uptake and secondary NfκB nuclear translocation. *Front. Immunol.* **2014**, *5*, 517. [[CrossRef](#)] [[PubMed](#)]
22. Li, J.; Lee, Y.; Johansson, H.J.; Mäger, I.; Vader, P.; Nordin, J.Z.; Wiklander, O.P.; Lehtiö, J.; Wood, M.J.; Andaloussi, S.E. Serum-free culture alters the quantity and protein composition of neuroblastoma-derived extracellular vesicles. *J. Extracell. Vesicles* **2015**, *4*, 26883. [[CrossRef](#)] [[PubMed](#)]
23. Di Noto, G.; Bugatti, A.; Zendrini, A.; Mazzoldi, E.L.; Montanelli, A.; Caimi, L.; Rusnati, M.; Ricotta, D.; Bergese, P. Merging colloidal nanoplasmonics and surface plasmon resonance spectroscopy for enhanced profiling of multiple myeloma-derived exosomes. *Biosens. Bioelectron.* **2016**, *77*, 518–524. [[CrossRef](#)] [[PubMed](#)]
24. Paolini, L.; Radeghieri, A.; Civini, S.; Caimi, L.; Ricotta, D. The Epsilon Hinge-Ear Region Regulates Membrane Localization of the AP-4 Complex. *Traffic* **2011**, *12*, 1604. [[CrossRef](#)] [[PubMed](#)]
25. Radeghieri, A.; Savio, G.; Zendrini, A.; Di Noto, G.; Salvi, A.; Bergese, P.; Piovani, G. Cultured human amniocytes express hTERT, which is distributed between nucleus and cytoplasm and is secreted in extracellular vesicles. *Biochem. Biophys. Res. Commun.* **2017**, *483*, 706–711. [[CrossRef](#)] [[PubMed](#)]
26. Horcas, L.; Fernandez, R. WSXM: A software for scanning probe microscopy and a tool for nanotechnology. *Rev. Sci. Instr.* **2007**, *78*, 013705. [[CrossRef](#)] [[PubMed](#)]
27. Stoney, G.G. The tension of metallic films deposited by electrolysis. *Proc. R. Soc. Lond. A* **1909**, *82*, 172. [[CrossRef](#)]
28. Van Eysden, C.A.; Sader, J.E. Resonant frequencies of a rectangular cantilever beam immersed in a fluid. *J. Appl. Phys.* **2006**, *100*, 114916. [[CrossRef](#)]
29. Braun, T.; Barwich, V.; Ghatkesar, M.K.; Bredekamp, A.H.; Gerber, C.; Hegner, M.; Lang, H.P. Micromechanical mass sensors for biomolecular detection in a physiological environment. *Phys. Rev. E* **2005**, *72*, 031907. [[CrossRef](#)] [[PubMed](#)]
30. Ghatnekar-Nilsson, S.; Lindahl, J.; Dahlin, A.; Stjernholm, T.; Jeppesen, S.; Höök, S.; Montelius, L. Phospholipid vesicle adsorption measured in situ with resonating cantilevers in a liquid cell. *Nanotechnology* **2005**, *16*, 1512–1516. [[CrossRef](#)]
31. Federici, S.; Padovani, F.; Poli, M.; Rodriguez, F.C.; Arosio, P.; Depero, L.E.; Bergese, P. Energetics of surface confined ferritin during iron loading. *Colloids Surface B Biointerfaces* **2016**, *145*, 520. [[CrossRef](#)] [[PubMed](#)]
32. Paolini, L.; Orizio, F.; Busatto, S.; Radeghieri, A.; Bresciani, R.; Bergese, P.; Monti, E. Exosomes Secreted by HeLa Cells Shuttle on Their Surface the Plasma Membrane-Associated Sialidase NEU3. *Biochemistry* **2017**, *5*, 6401–6408. [[CrossRef](#)] [[PubMed](#)]
33. Biavardi, E.; Biavardi, E.; Federici, S.; Tudisco, C.; Menozzi, D.; Massera, C.; Sottini, A.; Condorelli, G.G.; Bergese, P.; Dalcan, E. Cavitand-Grafted Silicon Microcantilevers as a Universal Probe for Illicit and Designer Drugs in Water. *Angew. Chem. Int. Ed.* **2014**, *53*, 9183–9188. [[CrossRef](#)] [[PubMed](#)]
34. Oliviero, G.; Federici, S.; Colombi, P.; Bergese, P. On the difference of equilibrium constants of DNA hybridization in bulk solution and at the solid-solution interface. *J. Mol. Recognit.* **2010**, *24*, 182–187. [[CrossRef](#)] [[PubMed](#)]
35. Bergese, P.; Oliviero, G.; Colombo, I.; Depero, L.E. Molecular recognition by contact angle: Proof of concept with DNA hybridization. *J. Surf. Coll.* **2009**, *25*, 4271–4273. [[CrossRef](#)] [[PubMed](#)]
36. Maiolo, D.; Mitola, S.; Leali, D.; Oliviero, G.; Ravelli, C.; Bugatti, A.; Depero, L.E.; Presta, M.; Bergese, P. Role of nanomechanics in canonical and noncanonical pro-angiogenic ligand/VEGF receptor-2 activation. *JACS* **2012**, *134*, 14573–14579. [[CrossRef](#)] [[PubMed](#)]
37. Federici, S.; Oliviero, G.; Hamad-Schifferli, K.; Bergese, P. Protein thin film machines. *Nanoscale* **2010**, *2*, 2570–2574. [[CrossRef](#)] [[PubMed](#)]
38. Braun, T.; Backmann, N.; Vöggtli, M.; Bietsch, A.; Engel, A.; Lang, H.-P.; Gerber, C.; Hegner, M. Conformational change of bacteriorhodopsin quantitatively monitored by microcantilever sensors. *Biophys. J.* **2006**, *90*, 2970–2977. [[CrossRef](#)] [[PubMed](#)]
39. Padovani, F.; Duffy, J.; Hegner, M. Nanomechanical clinical coagulation diagnostics and monitoring of therapies. *Nanoscale* **2017**, *9*, 17939–17947. [[CrossRef](#)] [[PubMed](#)]
40. Maiolo, D.; Federici, S.; Ravelli, L.; Depero, L.E.; Hamad-Schifferli, K.; Bergese, P. Nanomechanics of surface DNA switches probed by captive contact angle. *J. Colloid Interface Sci.* **2013**, *402*, 334–339. [[CrossRef](#)] [[PubMed](#)]

41. Longo, G.; Alonso-Sarduy, L.; Marques Rio, L.; Bizzini, A.; Trampuz, A.; Notz, J.; Dietler, G.; Kasas, S. Rapid detection of bacterial resistance to antibiotics using AFM cantilevers as nanomechanical sensors. *Nat. Nanotechnol.* **2013**, *8*, 522–526. [[CrossRef](#)] [[PubMed](#)]
42. Burg, T.; Godin, M.; Knudsen, S.M.; Shen, W.; Carlson, G.; Foster, J.S.; Babcock, K.; Manalis, S.R. Weighing of biomolecules, single cells and single nanoparticles in fluid. *Nature* **2007**, *446*, 1066–1069. [[CrossRef](#)] [[PubMed](#)]
43. Martínez-Martín, D.; Fläschner, G.; Gaub, B.; Martin, S.; Newton, R.; Beerli, C.; Mercer, J.; Gerber, C.; Müller, D.J. Inertial picobalance reveals fast mass fluctuations in mammalian cells. *Nature* **2017**, *550*, 500–505. [[CrossRef](#)] [[PubMed](#)]
44. Bergese, P.; Bontempia, E.; Chiarib, M.; Colombia, P.; Daminb, F.; Deperoa, L.E.; Olivieroa, G.; Pirrib, G.; Zuccaa, M. Investigation of a biofunctional polymeric coating deposited onto silicon microcantilevers. *Appl. Surface Sci.* **2007**, *253*, 4226–4231. [[CrossRef](#)]
45. Groves, J.T.; Ulman, N.; Boxer, S.G. Micropatterning fluid lipid bilayers on solid supports. *Science* **1997**, *275*, 651–653. [[CrossRef](#)] [[PubMed](#)]
46. Keller, C.A.; Glasmaster, K.; Zhdanov, V.P.; Kasemo, B. Formation of supported membranes from vesicles. *Phys. Rev. Lett.* **2000**, *84*, 5443–5446. [[CrossRef](#)] [[PubMed](#)]
47. Groves, J.T.; Ulman, N.; Cremer, P.S.; Boxer, S.G. Substrate–membrane interactions: Mechanisms for imposing patterns on a fluid bilayer membrane. *Langmuir* **1998**, *14*, 3347–3350. [[CrossRef](#)]
48. Sofou, S.; Thomas, J.L. Stable adhesion of phospholipid vesicles to modified gold surfaces. *Biosens. Bioelectron.* **2003**, *18*, 445–455. [[CrossRef](#)]
49. Kalyankar, N.D.; Sharma, M.K.; Vaidya, S.V.; Calhoun, D.; Maldarelli, C.; Couzis, A.; Gilchrist, L. Arraying of intact liposomes into chemically functionalized microwells. *Langmuir* **2006**, *22*, 5403–5411. [[CrossRef](#)] [[PubMed](#)]
50. Prime, K.L.; Whitesides, G.M. Adsorption of proteins onto surfaces containing end-attached oligo (ethylene oxide): A model system using self-assembled monolayers. *JACS* **1993**, *115*, 10714–10721. [[CrossRef](#)]
51. Gozen, I.; Jesorka, A. Instrumental methods to characterize molecular phospholipid films on solid supports. *Anal. Chem.* **2012**, *84*, 822–838. [[CrossRef](#)] [[PubMed](#)]
52. Hardy, G.J.; Nayak, R.; Zauscher, S. Model cell membranes: Techniques to form complex biomimetic supported lipid bilayers via vesicle fusion. *Curr. Opin. Colloid Interface Sci.* **2013**, *18*, 448–458. [[CrossRef](#)] [[PubMed](#)]
53. Van Weerd, J.; Karperien, M.; Jonkheijm, P. Supported lipid bilayers for the generation of dynamic cell–material interfaces. *Adv. Healthc. Mater.* **2015**, *4*, 2743–2779. [[CrossRef](#)] [[PubMed](#)]
54. Desplantes, R.; Lévêque, C.; Muller, B.; Lotierzo, M.; Ferracci, G.; Popoff, M.; Seagar, M.; Mamoun, R.; El Far, O. Affinity biosensors using recombinant native membrane proteins displayed on exosomes: Application to botulinum neurotoxin B receptor. *Sci. Rep.* **2017**, *7*, 1032. [[CrossRef](#)] [[PubMed](#)]
55. Fernandez-Trillo, F.; Grover, L.M.; Stephenson-Brown, A.; Harrison, P.; Mendes, P.M. Vesicles in nature and the laboratory: Elucidation of their biological properties and synthesis of increasingly complex synthetic vesicles. *Angew. Chem. Int. Ed.* **2017**, *129*, 3142–3160. [[CrossRef](#)] [[PubMed](#)]
56. Salvatore, A.; Montis, C.; Berti, D.; Baglioni, P. Multifunctional magnetoliposomes for sequential controlled release. *ACS Nano* **2016**, *10*, 7749–7760. [[CrossRef](#)] [[PubMed](#)]

